ACS APPLIED NANO MATERIALS

www.acsanm.org Article

Photocatalytic Nitroaromatic Prodrug Activation by Functionalized Gold Nanoclusters

Dajiao Cheng, Rong Liu, Limei Tian, Quan Zhou, Fushuang Niu, Yinghong Yue,* and Ke Hu*

Cite This: *ACS Appl. Nano Mater.* 2021, 4, 13413−13424 Read Online

ABSTRACT: Photocatalytic activation of prodrugs for killing cancer cells is an attractive alternative phototherapy to photodynamic therapy that typically relies on the supply of oxygen. Although prodrugs are widely developed, few other than Pt(IV) complexes are studied for photocatalytic activation. Herein, we report the photocatalytic reduction of nitrobenzene to aniline, an important chemical conversion for a large class of nitroaromatic prodrugs in cancer therapy that was previously limited to only enzyme-catalyzed activation. The carefully designed photocatalyst is a photosensitizer (PS)-functionalized gold nanocluster (Au NC) (abbreviated as Au-PS) in which a ruthenium coordination compound as the PS is covalently linked to the glutathione-ligated Au NC surface. Visible light excitation of the photocatalyst reduces nitrobenzene to aniline with 100% selectivity. The remarkably high selectivity is attributed to the specific catalytic nature of the reduced Au NC from photoinduced charge separation within the Au-PS analyzed by time-resolved absorption spectroscopy. *In vitro* experiments show that the nitroaromatic prodrug 5-(aziridin-1-yl)-2,4-dinitrobenzamide (CB1954) induces significant cytotoxicity in the presence of the Au-PS and light under hypoxia. The photocatalytic nitroaromatic prodrug activation by the Au-PS provides an alternative approach in the category of photochemotherapy to confront hypoxic cancer cells.

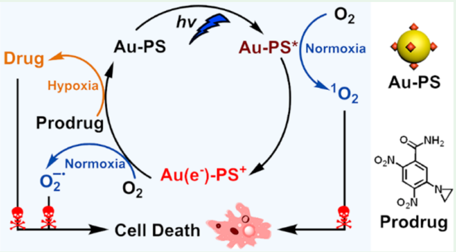

KEYWORDS: *gold nanocluster, photosensitizer, photocatalysis, prodrug, photochemotherapy*

■ INTRODUCTION

Photodynamic therapy (PDT) utilizes photogenerated reactive oxygen species (ROS) to kill cancer cells through the conversion of ground state molecular oxygen to either singlet oxygen or other ROS. Low concentration of molecular oxygen that is often found in solid tumors, however, limits the therapeutic efficacy of PDT.[1,2] This challenge has been tackled by a number of strategies including direct oxygen delivery by oxygen-carrying materials,[3,4] on-site oxygen generation by highly expressed hydrogen peroxide,[5−7] and the use of low oxygen-dependent photosensitizers (PSs),[8−10] just to name a few.

Photochemotherapy, on the other hand, has been a method of rising interest when low oxygen concentrations at cancerous sites become an issue because the method utilizes light to generate therapeutic drugs such as cisplatin and other related Pt(II) complexes.[11−14] In particular, photocatalytic prodrug activation is a further valuable advancement out of photochemotherapy as photocatalysts turnover target substrates with amplification, hence a reduction of necessary doses of activators such as PSs that could potentially cause side effects.[15−17] One of the shortcomings, however, lies in the limited choice of prodrugs and the corresponding product-specific photocatalysts. The only widely studied prodrugs by the photocatalytic activation method are Pt(IV) complexes as the active Pt(II) complexes can be relatively easy to generate through two-electron reduction by a number of PSs.[16−18]

To remedy the situation of scarcity, we turn to a class of nitroaromatic prodrugs. Nitroaromatics are a large class of prodrugs that can generate cytotoxic aromatic amines upon reduction.[19] These prodrugs are usually reduced by intracellularly overexpressed nitroreductases (NTRs) and are promisingly employed in gene-dependent enzyme prodrug therapy.[19,20] However, nitroaromatic prodrug activation is currently reliant on NTRs. Common artificial PSs are difficult to mimic these natural enzymes because a nitroaromatic requires challenging six electrons and six protons to transform to aromatic amine whereas the activation of Pt(IV)[13,21] only needs two electrons. Furthermore, unselective reductions would lead to other side products such as arylhydroxylamine or azoarenes, and so forth. With a careful design of the photocatalyst, nitroaromatic photoreduction could extend photocatalytic prodrug activation beyond Pt(IV) prodrugs.

Our previous work communicated the photocatalytic reduction of nitrobenzene (NB) based on glutathione (GSH)-ligand-stabilized gold nanocluster (Au NC) in the presence of the electron donor GSH *in vitro*.[22] This prior work

Received: September 14, 2021
Accepted: November 17, 2021
Published: November 25, 2021

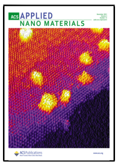

https://doi.org/10.1021/acsanm.1c02926
ACS Appl. Nano Mater. 2021, 4, 13413−13424

demonstrated that Au NC could perform the same catalytic function as nitroreductase with additional catalytic rate control from light irradiances. Along with high photostability, long-lived photoluminescent excited state, good dispersity, and excellent biocompatibility,[23] the Au NC is thereby an ideal fit as a photocatalyst for photocatalytic nitroaromatic prodrug activation in cancer cells. What is insufficient for the Au NC employed in the prior work is that it only absorbed very little blue light and had low photocatalytic efficiency.

In this study, we present the material characterization, photophysical and photocatalytic properties, and *in vitro* prodrug activation of a photocatalyst based on the covalently linked molecular PS to the Au NC (abbreviated as Au-PS), Scheme 1. The PS employed herein is the classic Ru(II) tris-bipyridine (bpy)-type coordination compound. The Ru(II) to bipyridine metal-to-ligand charge transfer (MLCT) band significantly extends the visible light absorption compared to the Au NC alone. We found that the MLCT excited state of the PS resulted in the charge-separated state Au(e^-)-PS$^+$ that was capable of multielectron transfer catalytic reduction of nitrobenzene to aniline with a remarkable 100% selectivity under hypoxic condition. The photocatalytic performance of the Au-PS was significantly improved compared to either the Au NC or Ru(bpy)$_3$Cl$_2$ alone. The improvement was attributed to the remarkable hundreds of milliseconds long lifetime of the charge-separated state Au(e^-)-PS$^+$. Under normoxic condition, the photoexcited PS of the Au-PS could either do energy transfer to produce singlet oxygen or reduce oxygen to generate other ROS such as superoxide. The generation of ROS and the photoactivation of the nitrobenzene moiety containing the nitroaromatic prodrug CB1954 catalyzed by the Au-PS lead to a dual killing mechanism for the death of cancer cells no matter whether the targeted cells are in hypoxic or normoxic condition. This study provides a new approach to complementing PDT and achieving selective nitroaromatic prodrug activation by photocatalysis when the cellular oxygen level is low.

Scheme 1. Proposed Mechanism of the Au-PS for Photodynamic and Photocatalytic Double Killing of Cancer Cells

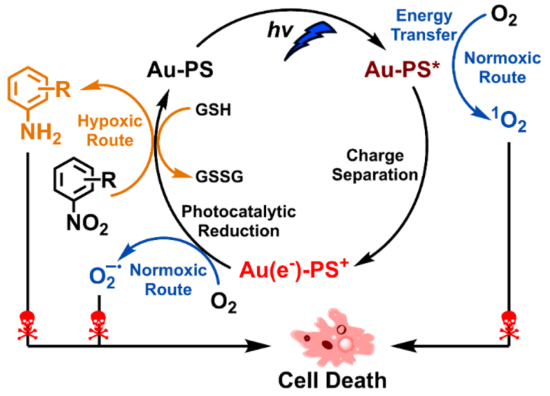

■ RESULTS AND DISCUSSION

Au-PS Synthesis and Characterization. The PS, [Ru(2,2′-bipyridyl)$_2$(4,4′-bis(bromomethyl)-2,2′-bipyridyl)]$^{2+}$, was covalently linked to the glutathione (GSH) ligand that stabilized the Au NC through the nucleophilic substitution reaction at room temperature, Figure 1a. The Au-PS was purified easily by centrifugation. The size of the Au-PS was about 1 nm in diameter as was observed by high-resolution transmission electron microscopy (HRTEM) (Figure 1b and inset in 1b). Figure 1c shows the ground state UV−vis absorption spectra of the PS, Au NC, and Au-PS, respectively. The absorption of the Au-PS can be approximated by a combination of the absorptions of the PS and Au NC. Absorption simulation from the combination of the PS and Au NC suggested on an average seven covalently linked PSs per

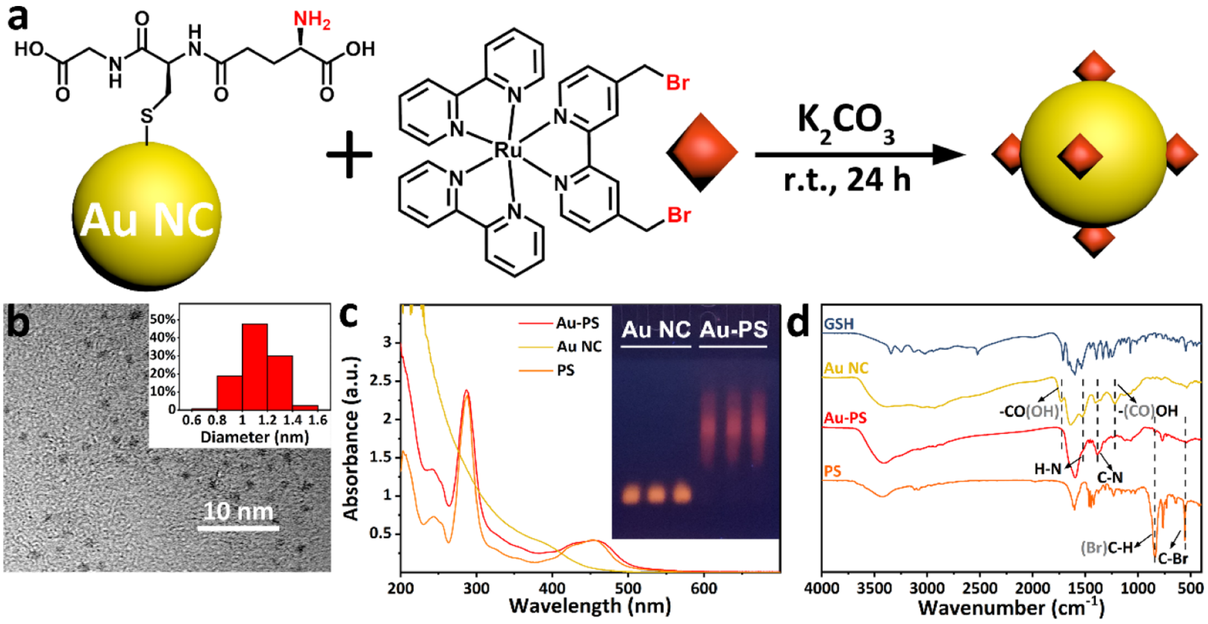

Figure 1. Synthesis and characterization of the Au-PS. (a) Schematic illustration of the preparation of the Au-PS. (b) HRTEM image of the Au-PS (Scale bar = 10 nm). Inset: Size distribution of the Au-PS. (c) UV−vis absorption spectra of the Au-PS, Au NC, and PS in DW. Inset: Au NC band and Au-PS band from the same tricine-SDS-PAGE under UV light. (d) FT-IR spectra of the GSH, Au NC, Au-PS, and PS.

https://doi.org/10.1021/acsanm.1c02926
ACS Appl. Nano Mater. 2021, 4, 13413−13424

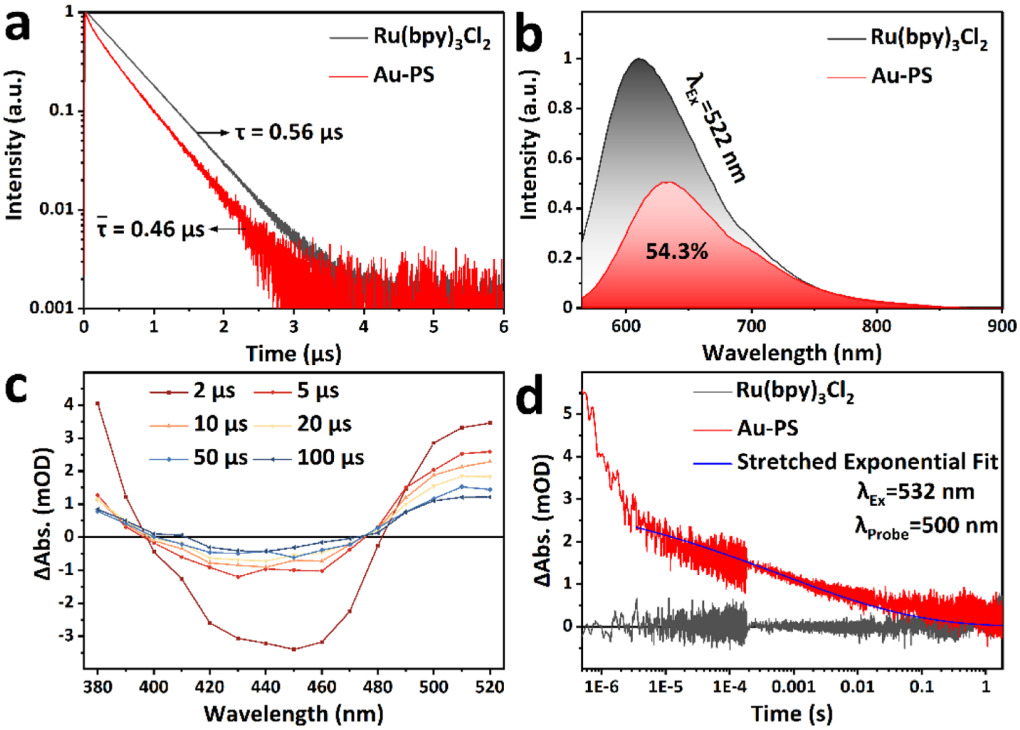

Figure 2. (a) Time-resolved photoluminescence decays of Ru(bpy)$_3$Cl$_2$ and the Au-PS following photoexcitation at 532 nm. (b) Steady state photoluminescence spectra of Ru(bpy)$_3$Cl$_2$ and the Au-PS following photoexcitation at 522 nm where ground state absorptions were the same. The number represents the ratio of the red region to the black region. (c) Transient absorption difference spectra of the Au-PS in aqueous solutions at indicated delay times after 532 nm pulsed laser excitation. (d) Absorption difference changes of the Au-PS and Ru(bpy)$_3$Cl$_2$ model sensitizer in aqueous solutions monitored at probe wavelengths of 500 nm as a function of logarithmic time after 532 nm pulsed laser excitation. The overlaid curve in blue is the stretched exponential fit to the kinetic data.

Au NC. This PS to Au NC linkage ratio was further confirmed by inductively coupled plasma-atomic emission spectroscopy (ICP-AES) that determined the molar ratio of elemental gold to ruthenium to be 4.4. This molar ratio translated to 6.5 PS molecules linking to a Au NC on average provided that Au NC maintained its molecular formula of Au$_{29}$(GSH)$_{27}$, which was in fairly good agreement with the ground state absorption simulation.

Tricine-sodium dodecyl sulfate-polyacrylamide gel electrophoresis (tricine-SDS-PAGE) was carried out to measure the molecular weight of the Au-PS. With the help of a black light, spots of the Au NC and Au-PS could be easily identified through their photoluminescence in orange and red, respectively, which was consistent with the photoluminescence spectra (Figure S1). The electrophoresis result showed that the mobility of the Au-PS was much lower than that of the Au NC (inset in Figure 1c). The lower mobility was the result of the larger molecular weight, which suggested the successful linkage between the Au NC and the PS.

The ^{1}H nuclear magnetic resonance (^{1}H NMR) spectrum of the Au-PS showed peaks of the aromatic protons at the same chemical shifts as the PS alone but with a significant line broadening (Figure S2). This ^{1}H NMR line broadening effect could be attributed to the loss of J-coupling information,[24] in support of the attachment of the PS molecules to the surface of the Au NC.

The successful incorporation of the PS with the Au NC was further characterized by Fourier transform infrared spectroscopy (FT-IR) to probe the molecular structural nature of this linkage (Figure 1d). Both the GSH-stabilized Au NC and pure GSH displayed peaks at 1726 cm^{-1} that belonged to the C═O stretching vibration of the carboxylic acid group from the amino acid residue. The peak disappeared in the Au-PS because both terminal carboxyl groups of GSH were deprotonated during the synthesis process.[25] For the same reason, there was also no O−H bending vibration peak in the Au-PS at 1226 cm^{-1}.[26] At the same time, we did not observe the C═O stretching vibration from the ester group in the Au-PS. Therefore, we inferred that the PS molecule did not react with the carboxyl group in the GSH ligand on the surface of the Au NC.

The amide bond peak at 1531 cm^{-1} (N−H bending) was stronger than that at 1397 cm^{-1} (C−N stretching) in the Au NC and GSH.[27] However, the peak of C−N stretching vibration at 1384 cm^{-1} was stronger in the Au-PS than the Au NC, which was ascribed to the formation of a new C−N bond in the Au-PS. The band at 557 cm^{-1} was assigned to the C−Br stretching vibration and that at 840 cm^{-1} was assigned to the C(Br)−H out-of-plane bending vibration in the PS. The PS was covalently linked to the Au NC by the benzyl bromide group as both of the two bromine atom related vibrational modes were gone after the formation of the Au-PS.[28] The FT-IR analysis further verified that the benzyl bromide group of the PS reacted and was covalently linked with the amino group of the GSH ligand on the surface of the Au NC to yield the Au-PS.

Photophysics of the Au-PS. As shown in Scheme 1, the PS molecules on the surface of the Au-PS were excited with either blue or green light from the ground state Au-PS to the excited state Au-PS*. Subsequently, a portion of the PS excited states injected electrons to the Au NC core to yield the charge-separated state Au(e$^-$)-PS$^+$ whereas the other PS excited states

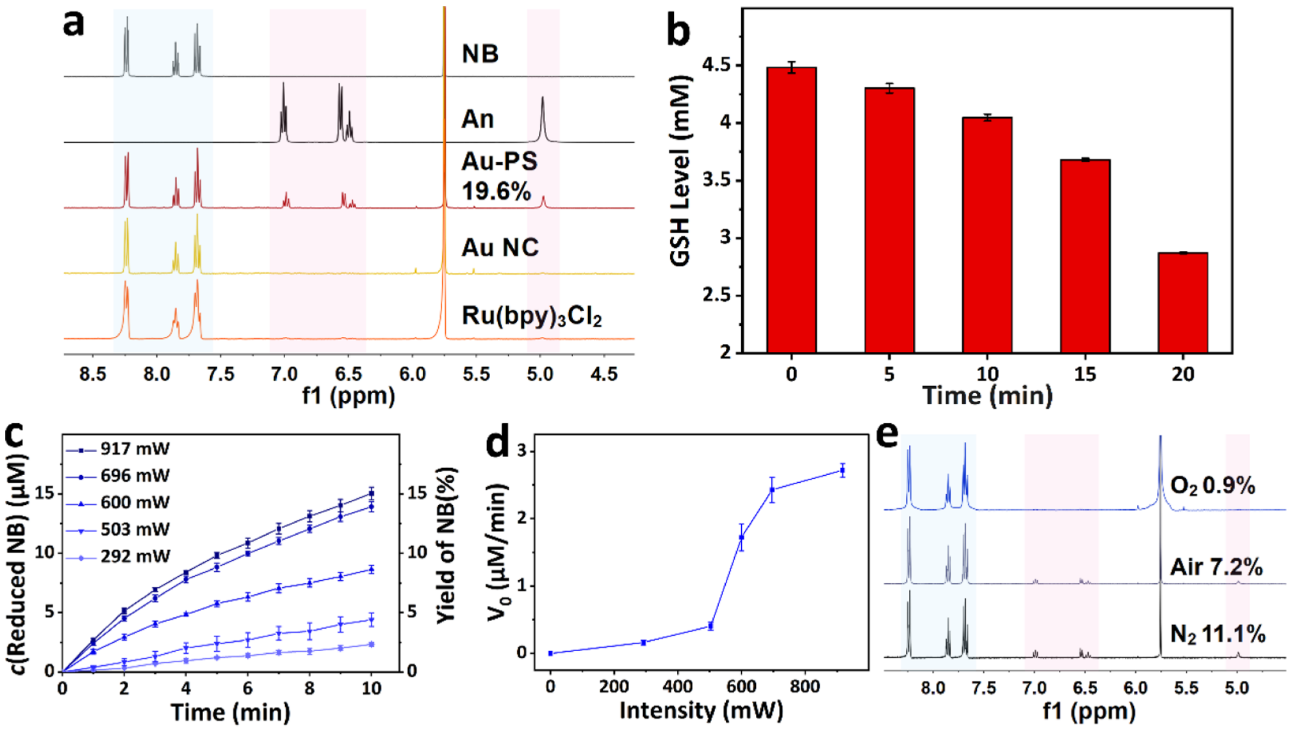

Figure 3. (a) ^{1}H NMR analysis of the photocatalytic reduction of nitrobenzene to aniline (An) by the Au-PS, Au NC, or Ru(bpy)$_3$Cl$_2$ after 532 nm light irradiation (900 mW, 30 min) under hypoxic condition. The yield of aniline after 30 min of irradiation was marked on the graph. (b) GSH level in the photoreduction system detected by 5,5″-Dithiobis-(2-nitrobenzoic acid. (c) Rate and (d) initial velocity of the photocatalytic reduction of nitrobenzene (100 μM) with 3.13 μM of the Au-PS monitored by an UV−vis spectrophotometer under different irradiances of 450 nm laser. (e) Photocatalytic conversion of nitrobenzene to aniline by the Au-PS under 450 nm (900 mW, 30 min) in nitrogen, air, or oxygen gas environment monitored by ^{1}H NMR spectroscopy. The yields of aniline after 30 min of irradiation are marked on the graph.

that did not inject electrons returned to the ground state through emission.

The photoluminescence lifetime measurements of Ru(bpy)$_3$Cl$_2$ and the Au-PS in fluid solution were carried out by monitoring the emission wavelength maximum at 610 nm following nanosecond pulsed laser excitation at 532 nm (Figure 2a). Ru(bpy)$_3$Cl$_2$ in aqueous solution showed single exponential photoluminescence decay with the characteristic lifetime constant of 0.56 μs whereas the Au-PS showed a biexponential photoluminescence decay with the average lifetime constant of 0.46 μs (τ_1 = 0.10 μs, τ_2 = 0.49 μs). The biexponential decay behavior was attributed to the PS excited state electron injection to the covalently linked Au NC that quenched the PS excited state. Steady state photoluminescence measurements showed that the photoluminescence intensity from the Au-PS was only 54.3% of that from the PS alone given the same absorption at the excitation wavelength of 522 nm (Figure 2b). The result indicated that 45.7% of the PS excited states were converted to the charge-separated state, Au(e$^-$)-PS$^+$. In comparison, Ru(bpy)$_3$Cl$_2$ retained 97.4% photoluminescence intensity when Ru(bpy)$_3$Cl$_2$ was simply mixed with the unmodified Au NC (Figure S3). Covalent linkage between the Au NC and PS was considered the key to the increased yield of photoinduced charge separation. The steady state photoluminescence measurements along with the lifetime study indicated a sensitization mechanism as sketched out in Scheme 1.

Photoluminescence measurements are the indirect means of probing photoinduced electron transfer as photoluminescence quenching could be caused by a variety of photophysical and photochemical processes. To obtain direct proof, nanosecond transient absorption spectroscopy was carried out to study the photogenerated intermediates of the Au-PS after pulsed laser excitation. The transient absorption spectrum of Ru(bpy)$_3$Cl$_2$ in deaerated aqueous solution showed a ground state bleach and a weak positive band in the long wavelength region as was previously observed in the literature.[29] The wavelength of 500 nm was the isosbestic point for Ru(bpy)$_3$Cl$_2$ where extinction coefficients of the ground state and the excited state were the same, resulting in no absorption change in the transient absorption spectrum. The transient absorption decay lifetime was the same as the photoluminescence decay throughout the probed wavelengths. Figure 2c shows the transient absorption spectrum of the Au-PS in deaerated aqueous solution at indicated delay times. Spectral data of earlier delay times can be found in Figure S4a. Though the majority of the transient absorption signals at sub-microsecond time delays resembled those of Ru(bpy)$_3$Cl$_2$, the spectra after 2 μs time delay showed significant differences. First, the isosbestic point moved from 490 to 475 nm, indicating a second intermediate other than the Ru(bpy)$_3$Cl$_2$ excited state. Second, the ground state bleach as well the positive transient signals lasted over 100 μs. These long-lived transients were neither from the Ru(bpy)$_3$Cl$_2$ excited state nor from the Au NC excited state (Figure S4b). Note that prior studies on the transient absorption spectroscopy of a variety of gold nanoclusters suggested very similar absorption profiles for the excited state and the reduced state.[30] Because the isosbestic point of the unsensitized Au NC transient absorption spectra was located at 405 nm, it was reasonably inferred that the hypochromic shift of the isosbestic point for the Au-PS transient absorption spectra was due to the PS excited state electron injection into the covalently linked Au

NC core, leaving the hole on the PS as evidenced by the long-lived ground state bleach.

Figure 2d shows the absorption difference change monitored at 500 nm where the transient absorption contribution from the PS excited state can be ignored. Therefore, the transient absorption signal was only from the charge-separated state, Au(e^-)-PS$^+$. Remarkably, the lifetime of the charge-separated state spanned from microseconds to almost a second. The kinetic decay cannot be well modeled by a single exponential function. Instead, it can be modeled by a stretched exponential or the Kohlrausch−William−Watts function, $\Delta\text{Abs} = A \exp(-t/\tau_0)^{\beta}$, where A is the pre-exponential factor and β is the stretch factor inversely related to the Lévy distribution.[31,32] The characteristic time constant t abstracted from the fitting function was as slow as 0.64 ms. The average time constant $\overline{t}$ calculated from the first moment of the Lévy distribution ($\overline{t} = t/\beta \times \Gamma(1/\beta)$) was as slow as 77 ms given a low β value of 0.2 that was characteristic of highly dispersive kinetics. This kinetic behavior was similar to those commonly observed at the sensitized metal oxide semiconductor interfaces where the injected electrons in the semiconductor diffused until they got trapped on the oxidized positive charge at the interface, causing highly dispersive kinetics.[33] In the Au-PS, the injected electrons were likely to hop among gold atoms within the nanocluster core and to recombine with the oxidized PS up till 1 s. This remarkable long lifetime of the reduced gold nanocluster from the photoinduced charge separation of the Au-PS opened a great opportunity for the Au NC photocatalysis as is further elaborated in the following sections.

Au-PS-Catalyzed Photoreduction of Nitrobenzene and ROS Generation. The photocatalytic reduction reaction catalyzed by the Au-PS was monitored by ^{1}H NMR spectroscopy as is shown in Figure 3a. The spectra of the reaction mixture were compared with the possible nitrobenzene reduction products. It was found that aniline was the only photoreduction product detected by ^{1}H NMR spectroscopy without other intermediates. In addition, aniline was not produced in the dark (Figure S5a) or in the absence of the catalyst (Figure S5b). Note that when the prodrug CB1954 was employed as the substrate, an additional unidentified side product was detected by ^{1}H NMR spectroscopy, Figure S6, which could be due to the side reactions with the reactive aziridinyl substituent. Nevertheless, the selectivity was attributed to the reduced Au NC that was capable of six election transfer toward the reduction of nitrobenzene.[22] The catalytic selectivity was also backed by prior mechanistic studies on the thermo-catalytic reduction of nitroaromatics by Au NCs in which the intermediates were adsorbed on the surface of Au NCs before being released into the solution.[34] Integration of the aniline peaks with respect to the unreacted nitrobenzene peaks showed the conversion yield of 19.6% after 532 nm irradiation for 30 min in the presence of the Au-PS. Higher yields of conversion were possible with prolonged irradiation as the absorption of the Au-PS barely changed within 30 min of irradiation. In contrast, reaction products were negligibly observed with either the Au NC or Ru(bpy)$_3$Cl$_2$ as the photocatalyst at the excitation wavelength of 532 nm (Figure 3a). Note that the concentration of Ru(bpy)$_3$Cl$_2$ was kept the same as the PS in the Au-PS by evaluating its UV−vis peak absorption where the Au NC was weakly absorbed.

It is unsurprising that the Au NC as the photocatalyst did not lead to significant photoproduct as it barely absorbed beyond 500 nm. What is remarkable is that the absorption by the PS only at 532 nm in the Au-PS led to the same photoproduct as was catalyzed by the Au NC with 405 nm excitation in our prior work. Therefore, the use of 532 nm excitation wavelength could rule out the possibility that the Au NC in the Au-PS was directly excited for the catalytic reduction of nitrobenzene. The same photoproduct from catalysis by the Au-PS can be rationalized by the aforementioned photoinduced charge separation within the Au-PS to form the reduced Au NC by which the reduction of nitrobenzene was catalyzed. The Au-PS essentially extended the light absorption to where the PS was absorbed whereas keeping the photocatalytic activity of the Au NC toward nitroaromatics. This is particularly useful as the sensitization technique decouples the optimization needs for both light absorption and the catalytic activity. It is very difficult to tune both light absorption and the right energetics with the Au NC itself because these two parameters are inherently correlated as demonstrated by a number of prior studies.[35] We managed to have the PS absorb a much larger visible spectrum than the Au NC and still maintain the photocatalytic activity with photoinduced charge separation. One notable observation was that the control catalyst Ru(bpy)$_3$Cl$_2$ was subject to photodegradation as evidenced by a significant change of the ground state absorption particularly in the visible region (Figure S7a). In stark contrast, the covalently linked PS in the Au-PS barely had ground state absorption changes, which might be due to the covalent functionalization that prevented the bipyridine ligand loss upon photoexcitation (Figure S7b).

Electron donation is an indispensable part to fulfill the catalytic cycle. We chose GSH as the electron donor because it is the most abundant in the mammalian cell environment with intracellular concentrations from 0.5 to 10 mM.[36] As shown in Figure 3b, the GSH level was decreased significantly during the photocatalytic reduction process. The result showed that the catalytic photoreduction of nitrobenzene by the Au-PS in hypoxia was accompanied by a large consumption of the electron donor GSH, which is known to be present in higher concentrations in cancer cells than in normal cells.[37]

The photoreduction rate of nitrobenzene can be finely tuned by the laser irradiance and was quantified by nitrobenzene absorption decrease at 267 nm (Figure S8a), where there was almost no aniline absorption. The excitation wavelength of 450 nm was used for photocatalysis because it was the best wavelength in terms of the large absorptivity for the Au-PS. As shown in Figure 3c, the rate of nitrobenzene conversion increased with the increase in the laser irradiance. Significantly, the plot of initial rate as a function of laser irradiance showed a dramatic increase of initial rates at around 500 mW instead of a linear relationship (Figure 3d). Hypothetically, a nitrobenzene molecule left the surface of the Au NC only when it was fully reduced to aniline so that no other intermediates were observed. The laser irradiance dependence of the photocatalytic rate may refer to the multielectron transfer mechanism in which the intermediates from the nitrobenzene reduction were surface immobilized until being fully converted to the 6-electron 6-proton reduction product, aniline. The pH-dependent study showed that decreasing the solution pH from 7.4 to 3.7 could increase the photocatalytic reaction rate by a factor of two (Figure S8b). The favorable acidic environment might suggest that the fully reduced product, aniline, was able to readily leave the Au NC surface and yield a vacant reaction site to the next nitrobenzene substrate once being protonated

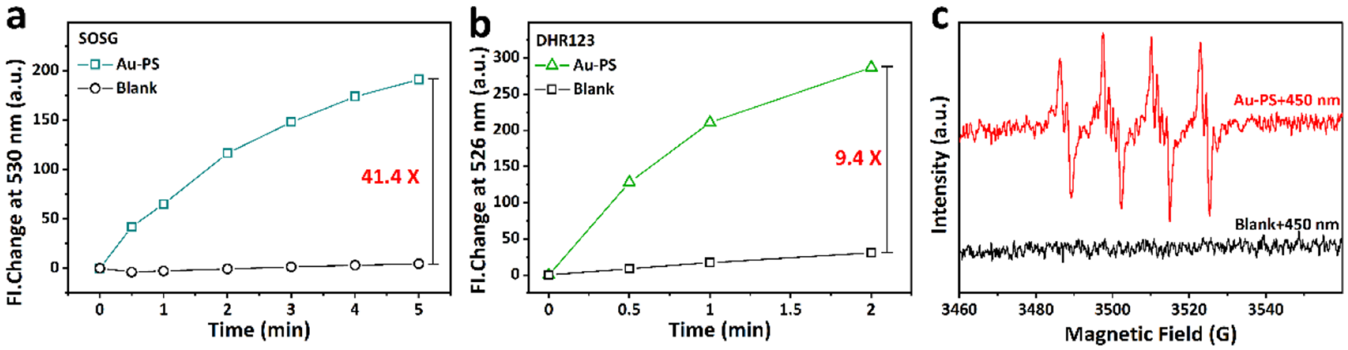

Figure 4. Fluorescence change of (a) SOSG at 530 nm and (b) DHR123 at 526 nm as a function of time when the indicated solution was irradiated by a 450 nm laser under ambient air. (c) EPR spectra of $O_2^{-\bullet}$ spin adduct (DMPO-OOH) in DMSO generated by the Au-PS under 450 nm light.

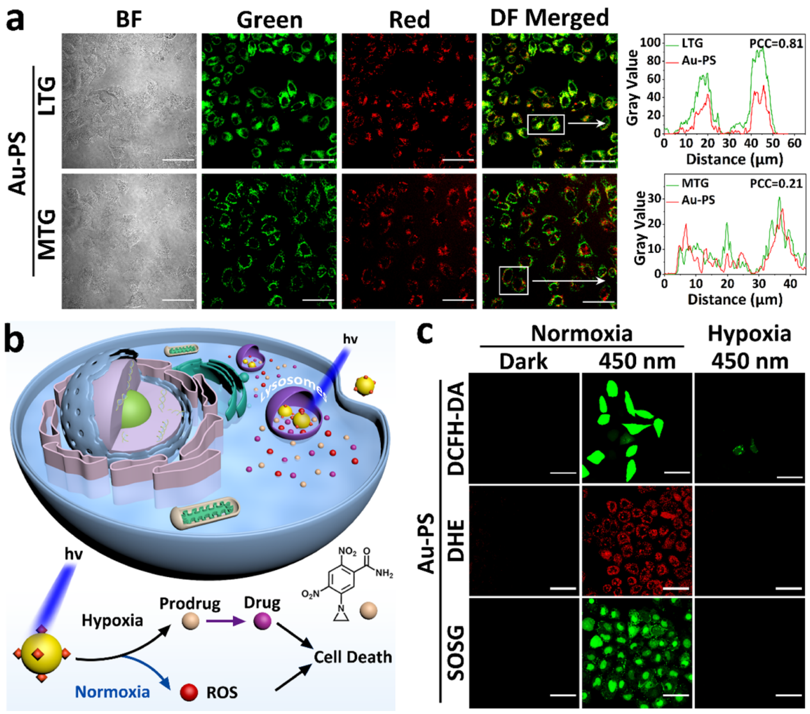

Figure 5. (a) Live-cell confocal luminescence imaging of the Au-PS co-stained with MTG or LTG in HeLa cells. Yellow shows the overlap of green and red. The intracellular fluorescence distribution and Pearson's correlation coefficient were from the cells located within the rectangles in white. (b) Schematic illustration of the photocatalytic reduction of the prodrug moiety nitrobenzene by the Au-PS with simultaneous ROS generation to induce cancer cell death. (c) ROS generated by the Au-PS including $^1O_2$ and $O_2^{-\bullet}$ in HeLa cells after 450 nm irradiation under normoxia and hypoxia, which was observed by confocal laser scanning microscopy. Scale bar = 50 μm.

and electrostatically repulsive to the positively charged PS at low pH conditions. This rationalization for the pH-dependent photocatalytic nitrobenzene reduction is consistent with a prior report using CdS quantum dots as the photocatalyst,[38] but a detailed study is out of the scope of this work and is subject to future studies. Besides being sensitive to the pH environment, the catalytic turnover was also controlled by the concentrations of nitrobenzene substrate (Figure S8c) and the indispensable GSH electron donor (Figures S8d and S9). Basically, higher substrate concentrations resulted in higher catalytic turnover frequencies that ranged from 20−70 h^{-1} or 120−420 electrons/Au-PS/h as plotted in Figure S10. This suggested an unsaturated catalytic activity by the Au-PS at biologically relevant substrate concentrations.

We further compared the photocatalytic nitrobenzene reduction yield with the Au-PS catalyst under variable oxygen concentration environment. ^1H NMR spectra of the reaction mixture after 30 min of light irradiation showed that the conversion yield of nitrobenzene was in the decreasing order under nitrogen, air, and pure oxygen atmosphere (Figure 3e). Ruthenium tris-bipyridine-type compounds are known to sensitize molecular oxygen to reactive singlet oxygen. We also discussed earlier in the section of photophysics of the Au-PS that less than half of the PS excited state formed the charge-separated state, Au(e^-)-PS^+. We envisioned that oxygen when present was expected to react primarily with the PS excited state.[39]

We then set out to test the ability of ROS generation photocatalyzed by the Au-PS under ambient air. The generation of singlet oxygen ($^1O_2$) by the Au-PS-containing solution, which was over 40-fold that with the blank sample, was detected by the singlet oxygen sensor green (SOSG), a

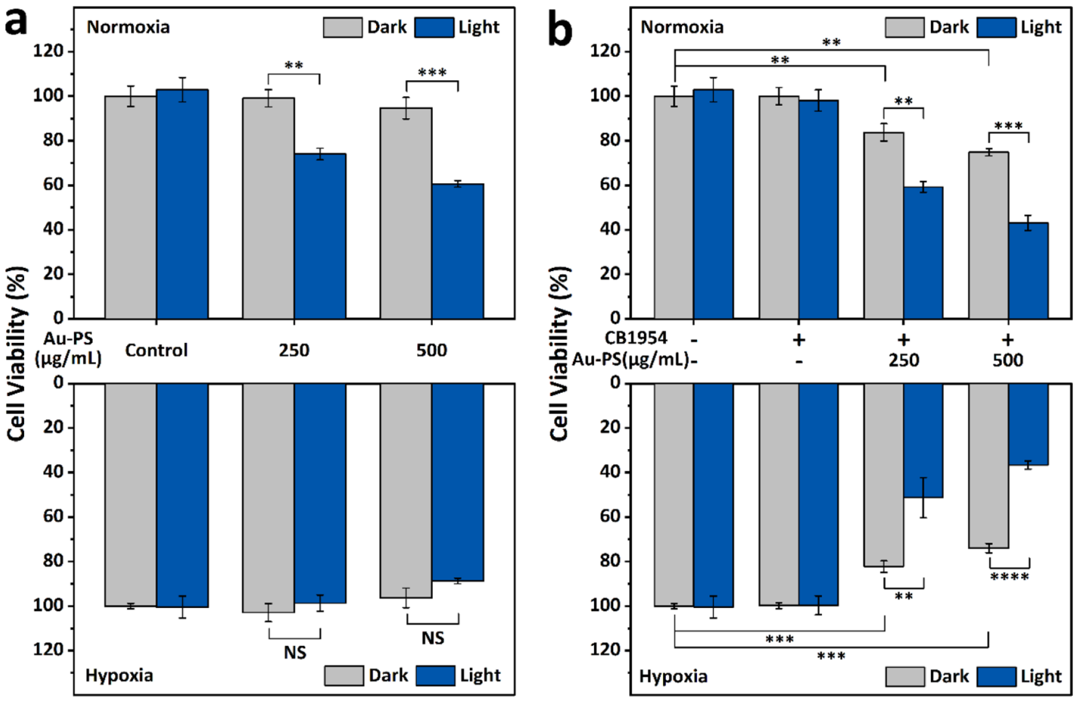

Figure 6. (a) Cell viability of HeLa cells incubated with different concentrations of the Au-PS under dark or light in normoxia and hypoxia. (b) Cytotoxicity of HeLa cells co-cultured with or without the Au-PS pretreatment followed with CB1954 in the dark or under irradiation in normoxia and hypoxia. For comparison, the control group was not co-incubated with the prodrug CB1954 and Au-PS. The data were expressed as mean ± S.D. $*P < 0.05$, $**P < 0.01$, $***P < 0.001$, and $****P < 0.0001$ determined by one-way ANOVA with Tukey post-test. $\alpha = 0.05$. NS stands for not significant.

fluorescence trap compound that turns on fluorescence after reaction with $^1O_2$ (Figure 4a).[40] The result indicated that the excited state of the Au-PS that did not convert to the charge-separated state could also play a role in PDT. The formation of a superoxide anion radical ($O_2^{-\bullet}$) was also detected by the 9.4-fold fluorescence intensity increase of the dihydrorhodamine123 (DHR123) molecular probe with the Au-PS present after irradiation, suggesting that the class I photodynamic process was also operative (Figure 4b).[8,41] Electron paramagnetic resonance (EPR) was employed to further confirm the generation of $O_2^{-\bullet}$ and 5,5-dimethyl-1-pyrroline-*N*-oxide (DMPO) was applied as the spin-trap agent. As shown in Figure 4c, the EPR signal of the $O_2^{-\bullet}$ spin adduct (DMPO-OOH) was observed in the presence of the Au-PS irradiated by a 450 nm laser under ambient air. The mechanism was likely that the Au(e$^-$)-PS$^+$ charge-separated state could also donate its electron to molecular oxygen because of favorable energetics [$E(\text{Au NC}^{0/-}) = -0.63$ V *vs* RHE, $E(O_2^{0/-\bullet}) = -0.16$ V *vs* NHE].[30,42]

Taken together, the Au-PS was capable of both class I and class II ROS generation for PDT when oxygen was abundant. Under hypoxic and acidic conditions prevalent in the tumor microenvironment,[43] the Au-PS was more efficient in carrying out the photocatalytic reduction of nitrobenzene to aniline.

Photoinduced Cytotoxicity under Normoxia and Hypoxia. The Au-PS was taken up by HeLa cells after being co-incubated for more than 9 h (Figure S11a) and remained stable in cell culture medium containing fetal bovine serum (FBS) (Figure S11b,c). The CCK8 cytotoxicity test showed that the Au-PS had a low dark cytotoxicity toward HeLa cells at 1 mg/mL after exposure for 24 h (Figure S11d), demonstrating its good biocompatibility. We employed a nitroaromatic prodrug CB1954 that had been through phase I clinical trials for gene therapy in the following *in vitro* experiments.[44] The toxicity of CB1954 with doses below 200 μM was negligible against HeLa cells after 3 h of drug exposure and recovery overnight (Figure S12). Furthermore, we investigated the intracellular distribution of the Au-PS co-staining with MitoTracker Green (MTG) and LysoTracker Green (LTG). As shown in Figure 5a, the Au-PS is localized in the lysosome, one of the ideal locations for PDT purposes.[45] Pearson's colocalization correlation coefficient of Au-PS with LTG was 0.81. A parallel colocalization experiment was also performed on the A549 cell line and showed similar Pearson's colocalization correlation coefficients either in lysosomes or mitochondria, Figure S13.

We further tested the phototoxicity against HeLa and A549 cancer cell lines due to the photoactivation of the prodrug CB1954 and the oxidative stress caused by the Au-PS as the process is pictorially shown in Figure 5b. When HeLa cells were only treated with the Au-PS for 12 h, there were ROS including $^1O_2$ and $O_2^{-\bullet}$ after light irradiation only under normoxia. They were detected by co-incubation with the specific probe 2′,7′-dichlorofluorescein-diacetate (DCFH-DA) (Figure S14), SOSG (Figure S15), and dihydroethidium (DHE) (Figure S16), respectively (Figure 5c).[46] Therefore cell viability was reduced after light irradiation only under normoxia (Figures 6a and S17a for A549). In contrast, extremely low phototoxicity was observed under hypoxia, indicating that the low concentration of molecular oxygen inside cancer cells limited the activity of the Au-PS. To overcome this drawback, the hypoxic condition can be exploited by introducing a redox active prodrug to convert to a cytotoxic species in hypoxic cancer cells.

Photocytotoxicity results as the prodrug CB1954 was employed. We have shown in our prior work that the photoexcited Au NC could activate CB1954 mainly in lysosomes and induce significant cytotoxicity.[22] However, phototoxicity was also caused by a 405 nm purple color excitation source that was required to excite a significant number of Au NCs. With the Au-PS as the photocatalyst, we were able to use green light or blue light of longer wavelengths. Here, 450 nm as the best wavelength of choice for photoexciting Au-PS was used in the cell experiment so that a lower light dose would be feasible to minimize the background phototoxicity while the catalytic effect would still be significant. Under dark or light irradiation, HeLa (Figure 6b) and A549 cells (Figure S17b) only co-cultured with low doses of CB1954 showed almost no cytotoxicity in either normoxic or hypoxic condition. When the Au-PS was co-incubated with the prodrug, there was a non-negligible amount of cell death in the dark. The reason is unknown but light irradiation induced a significant increase of cytotoxicity for HeLa and A549 cells under either normoxia or hypoxia. This finding verified our conjecture that the prodrug CB1954 was activated by the Au-PS under light irradiation in hypoxia, whereas the photocytotoxicity in normoxia was attributed to the simultaneous generation of ROS and the photocatalytic activation of CB1954. The Au-PS achieved the dual killing effect as was seen in a prior report with a Pt(IV) prodrug.[18]

One notable observation was that when the phototoxicity test was applied to a normal human liver cell line (HL-7702), the decrease of cell viability was insignificant no matter under dark/light or normoxic/hypoxic conditions, Figure S18. The photocatalytic reactions seemed to be selective toward cancer cells which was great but further investigation would be carried out on the origin of selectivity.

In addition, the apoptotic and dead cells were stained with Annexin V-FITC and propidium iodide (PI) separately in order to investigate the mechanism of cell death. The untreated HeLa cells under irradiation remained healthy with no significant staining with or without irradiation in normoxia and hypoxia (Figure S19). As shown in Figure S20, the non-irradiated cells treated with the Au-PS did not show any significant staining and had good cell viability. After 12 h of Au-PS exposure and light irradiation, HeLa cells growing under normoxia showed green and red fluorescence, indicating severe cell apoptosis and necrosis. Comparatively, the cells under hypoxia exhibited a less green fluorescence, supporting our conclusion that the concentration of intracellular molecular oxygen affected the PDT efficiency. In Figure S21, HeLa cells treated with the Au-PS and CB1954 without irradiation showed a faint green fluorescence indicating cell apoptosis. However, when HeLa cells were cultured with the Au-PS and prodrug CB1954 following irradiation and recovery overnight in normoxia and hypoxia, both of them showed a strong red fluorescence and weak green fluorescence. These results confirmed that CB1954 photo-reduced by the Au-PS induced apoptotic and necrotic cell death under hypoxic conditions and ROS generated by the Au-PS in normoxia also caused the same therapeutic effect.

■ CONCLUSIONS

In conclusion, we developed a method of synthesizing stable PS-functionalized gold nanocluster (Au-PS) with covalent linkage through a simple and facile one-pot reaction. The ruthenium tris-bipyridine-type PS absorbs visible light and transfers the triplet excited state to singlet oxygen when oxygen is abundant. When the oxygen concentration is low, the excited state PS injects an electron to the Au NC through photoinduced excited state charge transfer. The photo-reduced Au NC is remarkably long-lived and catalyzes the reduction of nitrobenzene to aniline with 100% selectivity and a turnover frequency as high as 70 h^{-1} under biologically relevant conditions. The Au-PS can therefore serve either as a PS for PDT application or as a photocatalyst that activates an aromatic nitro group containing the prodrug CB1954 in hypoxic cancer cells for photochemotherapy. The dual killing strategy enabled by the Au-PS overcomes the oxygen dependence of the traditional PDT and broadens the choice of early developed Pt(IV) prodrugs to more catalytic, selective, and demanding nitroaromatic prodrugs. Further modification on the red light absorption of the PS in the future would enable this dual killing strategy in animal tests.

■ EXPERIMENTAL SECTION

Materials and General Methods. *Materials.* $HAuCl_4 \cdot 3H_2O$, nitrobenzene, $RuCl_3$, 2,2′-bipyridine, LiCl, and 4,4′-bis-(bromomethyl)-2,2′-bipyridine were purchased from Aladdin (Shanghai, China). (5-(Aziridine-1-yl)-2,4-dinitrobenzamide) (CB1954) was synthesized according to literature methods.[22] The enhanced Cell Counting Kit-8, mitochondrial membrane potential assay kit with JC-1, ROS assay kit, DHE, MTG, and LTG were purchased from Beyotime Biotechnology (Shanghai, China). The Tricine-SDS-PAGE gel preparation kit, Annexin V-FITC/PI apoptosis detection kit, and Dulbecco's modified Eagle's medium were purchased from Sangon Biotechnology (Shanghai, China). SOSG reagent was purchased from Thermo Fisher Scientific.

Instruments. The absorption spectra were recorded on an Agilent Cary 60 UV−vis spectrophotometer. The fluorescence spectra were recorded on an Agilent Cary Eclipse fluorimeter. ^{1}H NMR spectra were recorded on a Bruker AVANCE III HD-400MHZ spectrometer. Luminescence imaging was performed on an Olympus FV-1000 laser confocal microscope. FT-IR spectra were obtained using a Thermo Fisher Nicolet iS10 IR spectrometer. The pH values were measured by a Mettler Toledo FiveEasy Plus pH meter. ICP-AES was detected on a PerkinElmer optical emission spectrometer (Optima-8000). Before the ICP-AES measurement, the Au-PS was digested in fresh aqua regia and then the solution was diluted with deionized water (DW) to detect the concentrations of gold and ruthenium. The tricine-SDS-PAGE was carried out on a VE-180 Mini-PROTEAN Tetra Cell (Tanon) to compare the molecular weights of the Au NC and Au-PS. The light used in the experiment was a blue diode laser at 450 nm and LD-pumped all-solid-state green laser at 532 nm (Changchun New Industries Optoelectronics Tech. Co. Ltd). The nanosecond transient absorption spectra were acquired on a TSP-2000 (Unisoku) laser flash photolysis system. Briefly, a Q-switched frequency-doubled pulsed Nd/YAG laser (Quantel Q-Smart 450, 10 Hz) was used as the excitation source to output 532 nm laser pulses (5−8 nm full width at half-maximum, 5 mJ/cm^2 per pulse). A 75 W Xenon arc lamp served as the probe beam that focused onto the solution sample in a 10 mm cuvette. The probe beam was aligned orthogonally to the excitation laser pulse and was passed into an f/300 mm monochromator (Acton, Princeton Instrument) that coupled a R2949 photomultiplier tube (Hamamatsu) to achieve signal detection. Transient absorption kinetic data at each wavelength were acquired on a computer interfaced digital oscilloscope (LeCroy 4024, 12 bit, 200 MHz) with typical 50−100 laser pulse averages. For transient photoluminescence data acquisition, the white light probe beam was blocked and the sample was only exposed to pulsed laser excitations. The signal detection was achieved in the same way as described above. Data were processed in Origin 9 and fit with least-squares error minimization using the Levenberg−Marquardt iteration method.

Synthesis and Characterization of [Ru^{II}(2,2′-bipyridyl)$_2$(4,4′-bis(bromomethyl)-2,2′-bipyridyl)](PF$_6$)$_2$ and the Au-PS. *Synthesis and Characterization of [Ru^{II}(2,2′-bipyridyl)$_2$(4,4′-bis-*

(bromomethyl)-2,2′-bipyridyl)](PF$_6$)$_2$ (PS). Synthesis of Ru^{II}(2,2′-bipyridyl)$_2$Cl$_2$·2H$_2$O. 2,2-Bipyridine (2.01 g, 12.57 mmol), LiCl (9.10, 18.86 mmol), and RuCl$_3$·6H$_2$O (1.319 g, 6.29 mmol) were dissolved in 250 mL of dimethylformamide (DMF) and refluxed for 8 h. After the solution was cooled to room temperature, 450 mL of acetone was added to the solution and the solid was precipitated. The obtained precipitate was filtered, washed, and dried. The desired product was purple solid with the yield of around 89%. ^{1}H NMR (400 MHz, DMSO-d_6): δ 9.98 (d, J = 5.61 Hz, 2H), 8.64 (d, J = 8.12 Hz, 2H), 8.48 (d, J = 8.12 Hz, 2H), 8.06 (t, J = 7.71 Hz, 2H), 7.77 (t, J = 6.61 Hz, 2H), 7.68 (t, J = 7.82 Hz, 2H), 7.51 (d, J = 5.71 Hz, 2H), and 7.10 (t, J = 6.61 Hz, 2H).

Synthesis of the PS. The compound Ru(bpy)$_2$Cl$_2$·2H$_2$O (1.07 g, 2.02 mmol) and silver triflate (1.07 g, 4.16 mmol) were dissolved in 9 mL of acetone and stirred for 8 h under N$_2$ at room temperature. Then, the precipitated AgCl was removed by filtration and 4,4′-bis(bromomethyl)-2,2′-bipyridine (0.69 g, 2.00 mmol) was added to the filtrate. After stirring for 2 h, the red solution was evaporated to dryness. The product was dissolved in H$_2$O and precipitated by the addition of aqueous NH$_4$PF$_6$. After drying, the crude product was recrystallized by dichloromethane (DCM)/ether and the desired product was dark red solid with the yield of around 62%. ^{1}H NMR (400 MHz, methanol-d_4): δ 8.78 (s, 2H), 8.70 (d, J = 8.22 Hz, 4H), 8.12 (t, J = 7.81 Hz, 4H), 7.81 (m, 6H), 7.55 (m, 2H), 7.50 (m, 4H), and 4.71 (s, 4H).

Synthesis of GSH-Modified Gold Nanoclusters (Au NCs). The synthesis of the Au NCs was based on the Xie group's work.[47] 250 mg of GSH was dissolved in DW (137.875 mL). Then, 2% tetrachloroauric acid aqueous solution (12.125 mL) was added to the above solution with vigorous stirring for about 1 h until the mixed solution became colorless at room temperature. The reaction system was further heated to 70 °C and stirred gently for 24 h. Next, the aqueous solution of Au NCs was condensed to 10 mL by rotary evaporation and subsequently mixed with acetone (20 mL) to precipitate Au NCs. The precipitate was collected by centrifugation at 8000 rpm for 10 min and washed with acetone three times. Finally, the Au NCs were redispersed in DW and freeze-dried to obtain the yellow powder.

Synthesis of the Au-PS. 4.5 mL of Au NC aqueous solution (4.6 mg/mL, pH = 7) was added to 10 mL of DW. 14.775 mL of the PS (2 mM, in CH$_3$OH) and 1.773 mL of K$_2$CO$_3$ aqueous solution (0.1 M) were mixed with the above solution. Then, the mixture was stirred gently (500 rpm) away from light for 24 h at room temperature. The solution was mixed with excess isopropanol and then centrifuged at 13,000 rpm for 15 min. The precipitate was redispersed in DW and isopropanol washing was repeated three times. In the end, the Au-PS was redispersed in DW and freeze-dried to obtain the product.

Tricine-SDS-PAGE. 10.6% separation gel was prepared by mixing 1.5 mL of 49.5% *T*, 6% *C*, 2.33 mL of gel buffer, 0.75 mL of glycerol, 2.42 mL of H$_2$O, 62 μL of 10% APS, and 6.5 μL of TEMED. The stacking gel and the eluting buffer were prepared according to the instruction of the tricine-SDS-PAGE gel preparation kit (Sangon Biotechnology). The samples were dissolved in a 50% (v/v) glycerol/water solution and then loaded onto the stacking gel (7.5 μL per well). The electrophoresis was allowed to run for about 3 h at a constant voltage mode (120 V) in an ice bath.

Photocatalytic Reactions by the Au-PS. *Photoreduction of Nitrobenzene under Hypoxia. ^{1}H NMR Spectra for the Photoreduction of NB.* 1 mL of Au-PS aqueous solution (4 mg/mL), 300 μL of NB (in CH$_3$OH, 140 mM), and 1 mL of GSH aqueous solution (150 mM) were mixed. 1.1 mL of the solution was taken out of the mixed system and degassed by bubbling nitrogen (N$_2$) for 15 min. One of them was on irradiation with 532 nm laser (900 mW) for 30 min and the other was in the dark. For comparison, the Au-PS was substituted by 760 μL of Ru(bpy)$_3$Cl$_2$ aqueous solution (2 mM) or 570 μL of Au NCs aqueous solution (4.6 mg/mL) and then DW was added to reach the volume of 2.3 mL. No materials were added in the blank control trial. After the illumination, 1 mL of the reaction solution, 1 mL of NaOH aqueous solution (2 M), and 1 mL of DCM were mixed thoroughly and the mixture stood for layering. After sucking out the upper solution, the lower one was blown with N$_2$ to volatilize DCM. Dimethyl sulfoxide-D6 (DMSO-D6) was added to dissolve the product later to be tested by ^{1}H NMR spectra. When the reaction system was irradiated with a 450 nm laser (900 mW) for 15 min, the amounts of materials were adjusted to 250 μL of Au-PS aqueous solution (2 mg/mL), 90 μL of Ru(bpy)$_3$Cl$_2$ aqueous solution (2 mM), and 70 μL of Au NCs aqueous solution (4.6 mg/mL).

The yield of nitrobenzene to aniline was measured to compare the photoreduction rate in nitrogen, air, and oxygen atmosphere and the experiment referred to the previous test.

UV−Vis Spectra for the Photoreaction of NB. In order to detect the factors affecting the photoreduction rate of NB, the following tests were performed. Generally, 50 μL of Au-PS aqueous solution (2 mg/mL) was added to 1.5 mL of phosphate-buffered saline (PBS) buffer containing NB (in DMSO, 10 mM) and GSH (in PBS, 100 mM). The reaction solution was blown into N$_2$ for 20 min and whereafter irradiated with a 450 nm laser for 10 min. During the reaction, the change of absorbance at 267 nm was monitored in real time by a UV−vis spectrophotometer, which represented the reduction of NB (ε_{267} = 8270 M^{-1}·cm^{-1}). The above experiments were repeated three times independently.

Photoreduction of O$_2$ under Normoxia. Detection of Superoxide Anion (O$_2^{-\bullet}$) with Dihydrorhodamine123 (DHR123). 3 μL of DHR123 (in DMSO, 5 mM) was mixed with 60 μL of Au-PS aqueous solution (2 mg/mL) in 1.5 mL of PBS buffer. While the reaction solution was irradiated with a 450 nm laser (59 mW), the fluorescence intensity of the probe was detected in real time (λ_{Ex} = 500 nm).

Detection of O$_2^{-\bullet}$ Using EPR. The O$_2^{-\bullet}$ generated by the Au-PS was further detected using the spin-trap agent, DMPO. 25 μL of DMPO (in DMSO, 0.2 M) was mixed with 1 μL of Au-PS aqueous solution (4 mg/mL) in 25 μL of DMSO. While the reaction solution was irradiated with a 450 nm laser (59 mW), the ESR signal was detected immediately.

Detection of Singlet Oxygen (^{1}O$_2$) with SOSG. 1.5 μL of SOSG (in CH$_3$OH, 5 mM) was added to 1.5 mL of PBS buffer containing 30 μL of Au-PS aqueous solution (2 mg/mL). The reaction solution was irradiated with a 450 nm laser (56 mW) and the fluorescence intensity of the probe was detected on a fluorescence spectrophotometer at the same time (λ_{Ex} = 504 nm).

Glutathione Consumption. 1 mL of PBS buffer contained 100 μL of Au-PS aqueous solution (2 mg/mL), 50 μL of NB (in DMSO, 10 mM), and 50 μL of GSH (in PBS, 100 mM). Nitrogen was bubbled into the solution for 15 min and the solution was shone under a 450 nm laser for 0−20 min. After that, the reaction solution was diluted six times with PBS buffer and the remaining GSH concentration was detected with 5,5′-dithiobis-(2-nitrobenzoic acid) by a Cytation 3 multi-mode microplate reader (BioTek).

***In Vitro* Test.** *Cell Culture.* HeLa cells (human cervical cancer), A549 cells (human pulmonary carcinoma), and HL-7702 (normal human liver) were cultured in DMEM media containing 10% FBS at 37 °C with 5% CO$_2$. They were grown in a T25 flask and cultured overnight before the experiment. Furthermore, in order to mimic the hypoxic tumor environment, the inoculated plates were placed in a 2.5 L anaerobic cultivation pot (Mitsubishi Gas Chemical, Japan) with oxygen-absorbing, carbon dioxide-generating AnaeroPack-Anaero sachets (MGC, Japan) according to the manufacturer's instruction and subsequently cultivated for another 3 h at 37 °C.

Cytotoxicity Test. HeLa cells were seeded in 96-well plates overnight and then incubated with the Au-PS at a concentration of 62.5, 125, 250, 500, and 1000 μg/mL for 24 h. After that, the Au-PS solution was removed out and then enhanced CCK8 was added into each well. The absorption at 450 nm of enhanced CCK8 was detected using a multi-mode microplate reader. A similar protocol was used for the dark cytotoxicity assay of CB1954 in HeLa cells.

For the photocytotoxicity test, HeLa cells were plated onto 96-well plates for 12 h and subsequently treated with or without the Au-PS (250 or 500 μg/mL) for 12 h. Thereafter, the culture medium was aspirated, and HeLa cells were then incubated in the presence or absence of the prodrug CB1954 (200 μM) for 3 h. Then, the cells were further incubated for 3 h under normoxic or hypoxic conditions and irradiated using a 450 nm laser (3 min, 9 J/cm^2) under respective conditions. After overnight incubation, enhanced CCK8 was added and cell viability was detected on the base of the protocols. For the dark cytotoxicity test, the light irradiation step was canceled and other steps were consistent with those described above. The same experiments were repeated in A549 cells and HL-7702 cells.

Cellular Uptake. HeLa cells were seeded into 6-well plates with cell climbing slices and incubated overnight. The Au-PS (1 mg/mL) was added to each well and cultured for 6, 9, and 12 h. After HeLa cells were washed with PBS three times, the fluorescence signals of the Au-PS were detected by laser confocal microscopy (excited at 488 nm, monitored at 620 ± 50 nm).

Intracellular Localization. HeLa cells were grown on 6-well plates with cell climbing slices for 12 h to achieve a stable attachment. Then, the Au-PS (500 μg/mL) was added and incubated for another 12 h. After that, the Au-PS was aspirated and the cells were rinsed three times with PBS. In order to analyze the cellular location of the Au-PS, HeLa cells were then stained by LTG or MTG for 30 min. The Au-PS was replaced with a new medium and its localization was detected using a laser confocal microscope. The excitation wavelength for the Au-PS, LTG, and MTG was 488 nm. The emission wavelength was collected from 600 to 700 nm for the Au-PS whereas from 490 to 520 nm for LTG and MTG. The same experiment was repeated in A549 cells.

Annexin V-FITC/PI Double-Staining for Apoptosis Detection. The Annexin V-FITC/PI apoptosis detection kit was employed to measure apoptosis in different treatment conditions. HeLa cells were placed in 6-well plates with cell climbing slices for 12 h and subsequently treated with or without the Au-PS (500 μg/mL) for 12 h. HeLa cells were then washed three times with PBS and incubated in the presence or absence of the prodrug CB1954 (200 μM) for another 3 h. After that, plates were incubated in normoxia or hypoxia for 3 h. The experimental groups were then irradiated with a 450 nm laser (3 min, 9 J/cm^2) under respective conditions and the control groups were left under dark. After overnight incubation, HeLa cells were double-stained with Annexin V-FITC and PI, imaged by a laser confocal microscope (Annexin V-FITC: λ_{Ex} = 488 nm, λ_{Em} = 500−570 nm; PI: λ_{Ex} = 543 nm, and λ_{Em} = 600−700 nm).

Intracellular Detection of ROS, $O_2^{-\bullet}$, and $^1O_2$. HeLa cells were seeded into 6-well plates with cell climbing slices for 12 h and subsequently treated with or without the Au-PS for 12 h. The Au-PS solution was then aspirated and washed three times with PBS. After that, cells were incubated in normoxia or hypoxia for 3 h and irradiated using a 450 nm laser (3 min, 9 J/cm^2) under respective conditions. Finally, DCFH-DA, DHE, and SOSG were used to assess the intracellular ROS, $O_2^{-\bullet}$, and $^1O_2$ level, respectively. The fluorescence signals were detected by laser confocal microscopy (DCFH-DA: λ_{Ex} = 488 nm, λ_{Em} = 500−540 nm; DHE: λ_{Ex} = 543 nm, λ_{Em} = 580−640 nm; SOSG: λ_{Ex} = 488 nm, and λ_{Em} = 500−550 nm).

■ ASSOCIATED CONTENT

Supporting Information

The Supporting Information is available free of charge at https://pubs.acs.org/doi/10.1021/acsanm.1c02926.

> Additional UV−vis, photoluminescence, ^{1}H NMR, and transient absorption spectra, NB photoreduction under different reaction conditions, turnover frequency as a function of time, additional cytotoxicity data, confocal laser scanning microscopy images of intercellular ROS level, and cell apoptosis analysis by Annexin V-FITC/PI staining (PDF)

■ AUTHOR INFORMATION

Corresponding Authors

Yinghong Yue − *Department of Chemistry, Fudan University, Shanghai 200433, P. R. China;* orcid.org/0000-0002-8000-1606; Email: yhyue@fudan.edu.cn

Ke Hu − *Department of Chemistry, Fudan University, Shanghai 200433, P. R. China;* orcid.org/0000-0002-0240-7192; Email: khu@fudan.edu.cn

Authors

Dajiao Cheng − *Department of Chemistry, Fudan University, Shanghai 200433, P. R. China*

Rong Liu − *Department of Chemistry, Fudan University, Shanghai 200433, P. R. China*

Limei Tian − *Department of Chemistry, Fudan University, Shanghai 200433, P. R. China*

Quan Zhou − *Department of Chemistry, Fudan University, Shanghai 200433, P. R. China*

Fushuang Niu − *Department of Chemistry, Fudan University, Shanghai 200433, P. R. China*

Complete contact information is available at:
https://pubs.acs.org/10.1021/acsanm.1c02926

Notes

The authors declare no competing financial interest.

■ ACKNOWLEDGMENTS

This work was sponsored by the National Natural Science Foundation of China (21872037) and Natural Science Foundation of Shanghai (21ZR1404400). K.H. also thanks Professor Tao Yi at Donghua University, Shanghai for valuable discussion during the preparation of the manuscript.

■ REFERENCES

(1) Liu, Y.; Jiang, Y.; Zhang, M.; Tang, Z.; He, M.; Bu, W. Modulating Hypoxia via Nanomaterials Chemistry for Efficient Treatment of Solid Tumors. *Acc. Chem. Res.* **2018**, *51*, 2502−2511.

(2) Li, X.; Kwon, N.; Guo, T.; Liu, Z.; Yoon, J. Innovative Strategies for Hypoxic-Tumor Photodynamic Therapy. *Angew. Chem., Int. Ed.* **2018**, *57*, 11522−11531.

(3) Song, G.; Liang, C.; Yi, X.; Zhao, Q.; Cheng, L.; Yang, K.; Liu, Z. Perfluorocarbon-Loaded Hollow Bi2Se3 Nanoparticles for Timely Supply of Oxygen under Near-Infrared Light to Enhance the Radiotherapy of Cancer. *Adv. Mater.* **2016**, *28*, 2716−2723.

(4) Cheng, Y.; Cheng, H.; Jiang, C.; Qiu, X.; Wang, K.; Huan, W.; Yuan, A.; Wu, J.; Hu, Y. Perfluorocarbon nanoparticles enhance reactive oxygen levels and tumour growth inhibition in photodynamic therapy. *Nat. Commun.* **2015**, *6*, 8785.

(5) Yao, C.; Wang, W.; Wang, P.; Zhao, M.; Li, X.; Zhang, F. Near-Infrared Upconversion Mesoporous Cerium Oxide Hollow Biophotocatalyst for Concurrent pH-/H2O2-Responsive O2-Evolving Synergetic Cancer Therapy. *Adv. Mater.* **2018**, *30*, 1704833.

(6) Zhu, W.; Dong, Z.; Fu, T.; Liu, J.; Chen, Q.; Li, Y.; Zhu, R.; Xu, L.; Liu, Z. Modulation of Hypoxia in Solid Tumor Microenvironment with MnO2 Nanoparticles to Enhance Photodynamic Therapy. *Adv. Funct. Mater.* **2016**, *26*, 5490−5498.

(7) Chen, W.; Sun, Z.; Jiang, C.; Sun, W.; Yu, B.; Wang, W.; Lu, L. An All-in-One Organic Semiconductor for Targeted Photoxidation Catalysis in Hypoxic Tumor. *Angew. Chem., Int. Ed.* **2021**, *60*, 16641−16648.

(8) Li, M.; Xia, J.; Tian, R.; Wang, J.; Fan, J.; Du, J.; Long, S.; Song, X.; Foley, J. W.; Peng, X. Near-Infrared Light-Initiated Molecular Superoxide Radical Generator: Rejuvenating Photodynamic Therapy against Hypoxic Tumors. *J. Am. Chem. Soc.* **2018**, *140*, 14851−14859.

(9) Huang, H.; Banerjee, S.; Qiu, K.; Zhang, P.; Blacque, O.; Malcomson, T.; Paterson, M. J.; Clarkson, G. J.; Staniforth, M.; Stavros, V. G.; Gasser, G.; Chao, H.; Sadler, P. J. Targeted photoredox catalysis in cancer cells. *Nat. Chem.* **2019**, *11*, 1041−1048.

(10) Lv, W.; Zhang, Z.; Zhang, K. Y.; Yang, H.; Liu, S.; Xu, A.; Guo, S.; Zhao, Q.; Huang, W. A Mitochondria-Targeted Photosensitizer

Showing Improved Photodynamic Therapy Effects Under Hypoxia. *Angew. Chem., Int. Ed.* **2016**, *55*, 9947−9951.

(11) Johnstone, T. C.; Suntharalingam, K.; Lippard, S. J. The Next Generation of Platinum Drugs: Targeted Pt(II) Agents, Nanoparticle Delivery, and Pt(IV) Prodrugs. *Chem. Rev.* **2016**, *116*, 3436−3486.

(12) Farrer, N. J.; Woods, J. A.; Salassa, L.; Zhao, Y.; Robinson, K. S.; Clarkson, G.; Mackay, F. S.; Sadler, P. J. A potent trans-diimine platinum anticancer complex photoactivated by visible light. *Angew. Chem., Int. Ed.* **2010**, *49*, 8905−8908.

(13) Wang, Z.; Wang, N.; Cheng, S.-C.; Xu, K.; Deng, Z.; Chen, S.; Xu, Z.; Xie, K.; Tse, M.-K.; Shi, P.; Hirao, H.; Ko, C.-C.; Zhu, G. Phorbiplatin, a Highly Potent Pt(IV) Antitumor Prodrug That Can Be Controllably Activated by Red Light. *Chem* **2019**, *5*, 3151−3165.

(14) Deng, Z.; Li, C.; Chen, S.; Zhou, Q.; Xu, Z.; Wang, Z.; Yao, H.; Hirao, H.; Zhu, G. An intramolecular photoswitch can significantly promote photoactivation of Pt(iv) prodrugs. *Chem. Sci.* **2021**, *12*, 6536.

(15) Soldevila-Barreda, J. J.; Metzler-Nolte, N. Intracellular Catalysis with Selected Metal Complexes and Metallic Nanoparticles: Advances toward the Development of Catalytic Metallodrugs. *Chem. Rev.* **2019**, *119*, 829−869.

(16) Gurruchaga-Pereda, J.; Martínez-Martínez, V.; Rezabal, E.; Lopez, X.; Garino, C.; Mancin, F.; Cortajarena, A. L.; Salassa, L. Flavin Bioorthogonal Photocatalysis Toward Platinum Substrates. *ACS Catal.* **2020**, *10*, 187−196.

(17) Mazzei, L. F.; Martínez, Á.; Trevisan, L.; Rosa-Gastaldo, D.; Cortajarena, A. L.; Mancin, F.; Salassa, L. Toward supramolecular nanozymes for the photocatalytic activation of Pt(iv) anticancer prodrugs. *Chem. Commun.* **2020**, *56*, 10461−10464.

(18) Norman, D. J.; Gambardella, A.; Mount, A. R.; Murray, A. F.; Bradley, M. A Dual Killing Strategy: Photocatalytic Generation of Singlet Oxygen with Concomitant PtIV Prodrug Activation. *Angew. Chem., Int. Ed.* **2019**, *58*, 14189−14192.

(19) Sharma, A.; Arambula, J. F.; Koo, S.; Kumar, R.; Singh, H.; Sessler, J. L.; Kim, J. S. Hypoxia-targeted drug delivery. *Chem. Soc. Rev.* **2019**, *48*, 771−813.

(20) Williams, E. M.; Little, R. F.; Mowday, A. M.; Rich, M. H.; Chan-Hyams, J. V. E.; Copp, J. N.; Smaill, J. B.; Patterson, A. V.; Ackerley, D. F.; Ackerley, D. F. Nitroreductase gene-directed enzyme prodrug therapy: insights and advances toward clinical utility. *Biochem. J.* **2015**, *471*, 131−153.

(21) Zhang, J. Z.; Wexselblatt, E.; Hambley, T. W.; Gibson, D. Pt(IV) analogs of oxaliplatin that do not follow the expected correlation between electrochemical reduction potential and rate of reduction by ascorbate. *Chem. Commun.* **2012**, *48*, 847−849.

(22) Liu, R.; Cheng, D.; Zhou, Q.; Niu, F.; Hu, K. Gold Nanoclusters Perform Enzyme-like Photocatalysis for Prodrug Activation. *ACS Appl. Nano Mater.* **2021**, *4*, 990−994.

(23) Yang, J.; Wang, F.; Yuan, H.; Zhang, L.; Jiang, Y.; Zhang, X.; Liu, C.; Chai, L.; Li, H.; Stenzel, M. Recent advances in ultra-small fluorescent Au nanoclusters toward oncological research. *Nanoscale* **2019**, *11*, 17967−17980.

(24) Wu, Z.; Gayathri, C.; Gil, R. R.; Jin, R. Probing the Structure and Charge State of Glutathione-Capped Au25(SG)18 Clusters by NMR and Mass Spectrometry. *J. Am. Chem. Soc.* **2009**, *131*, 6535−6542.

(25) Liu, Y.; Ma, W.; Liu, W.; Li, C.; Liu, Y.; Jiang, X.; Tang, Z. Silver(i)−glutathione biocoordination polymer hydrogel: effective antibacterial activity and improved cytocompatibility. *J. Mater. Chem.* **2011**, *21*, 19214−19218.

(26) Yang, Y.; Wang, S.; Chen, S.; Shen, Y.; Zhu, M. Switching the subcellular organelle targeting of atomically precise gold nanoclusters by modifying the capping ligand. *Chem. Commun.* **2018**, *54*, 9222−9225.

(27) Cui, X.; Wang, J.; Liu, B.; Ling, S.; Long, R.; Xiong, Y. Turning Au Nanoclusters Catalytically Active for Visible-Light-Driven CO2 Reduction through Bridging Ligands. *J. Am. Chem. Soc.* **2018**, *140*, 16514−16520.

(28) Govindarajan, M.; Periandy, S.; Carthigayen, K. FT-IR and FT-Raman spectra, thermo dynamical behavior, HOMO and LUMO, UV, NLO properties, computed frequency estimation analysis and electronic structure calculations on alpha-bromotoluene. *Spectrochim. Acta, Part A* **2012**, *97*, 411−422.

(29) Jian, J.-X.; Ye, C.; Wang, X.-Z.; Wen, M.; Li, Z.-J.; Li, X.-B.; Chen, B.; Tung, C.-H.; Wu, L.-Z. Comparison of H2 photogeneration by [FeFe]-hydrogenase mimics with CdSe QDs and Ru(bpy)3Cl2 in aqueous solution. *Energy Environ. Sci.* **2016**, *9*, 2083−2089.

(30) Stamplecoskie, K. G.; Chen, Y.-S.; Kamat, P. V. Excited-State Behavior of Luminescent Glutathione-Protected Gold Clusters. *J. Phys. Chem. C* **2014**, *118*, 1370−1376.

(31) Williams, G.; Watts, D. C. Non-symmetrical dielectric relaxation behaviour arising from a simple empirical decay function. *Trans. Faraday Soc.* **1970**, *66*, 80−85.

(32) Lindsey, C. P.; Patterson, G. D. Detailed comparison of the Williams–Watts and Cole–Davidson functions. *J. Chem. Phys.* **1980**, *73*, 3348−3357.

(33) Barzykin, A. V.; Tachiya, M. Mechanism of Charge Recombination in Dye-Sensitized Nanocrystalline Semiconductors:-Random Flight Model. *J. Phys. Chem. B* **2002**, *106*, 4356−4363.

(34) Wunder, S.; Polzer, F.; Lu, Y.; Mei, Y.; Ballauff, M. Kinetic Analysis of Catalytic Reduction of 4-Nitrophenol by Metallic Nanoparticles Immobilized in Spherical Polyelectrolyte Brushes. *J. Phys. Chem. C* **2010**, *114*, 8814−8820.

(35) Abbas, M. A.; Kamat, P. V.; Bang, J. H. Thiolated Gold Nanoclusters for Light Energy Conversion. *ACS Energy Lett.* **2018**, *3*, 840−854.

(36) Wu, G.; Fang, Y.-Z.; Yang, S.; Lupton, J. R.; Turner, N. D. Glutathione metabolism and its implications for health. *J. Nutr.* **2004**, *134*, 489−492.

(37) Zeng, L.; Kuang, S.; Li, G.; Jin, C.; Ji, L.; Chao, H. A GSH-activatable ruthenium(ii)-azo photosensitizer for two-photon photodynamic therapy. *Chem. Commun.* **2017**, *53*, 1977−1980.

(38) Jensen, S. C.; Homan, S. B.; Weiss, E. A. Photocatalytic Conversion of Nitrobenzene to Aniline through Sequential Proton-Coupled One-Electron Transfers from a Cadmium Sulfide Quantum Dot. *J. Am. Chem. Soc.* **2016**, *138*, 1591.

(39) Mari, C.; Pierroz, V.; Rubbiani, R.; Patra, M.; Hess, J.; Spingler, B.; Oehninger, L.; Schur, J.; Ott, I.; Salassa, L.; Ferrari, S.; Gasser, G. DNA intercalating Ru(II) polypyridyl complexes as effective photosensitizers in photodynamic therapy. *Chem.—Eur. J.* **2014**, *20*, 14421−14436.

(40) Zhao, X.; Long, S.; Li, M.; Cao, J.; Li, Y.; Guo, L.; Sun, W.; Du, J.; Fan, J.; Peng, X. Oxygen-Dependent Regulation of Excited-State Deactivation Process of Rational Photosensitizer for Smart Phototherapy. *J. Am. Chem. Soc.* **2020**, *142*, 1510−1517.

(41) Novohradsky, V.; Rovira, A.; Hally, C.; Galindo, A.; Vigueras, G.; Gandioso, A.; Svitelova, M.; Bresolí-Obach, R.; Kostrhunova, H.; Markova, L.; Kasparkova, J.; Nonell, S.; Ruiz, J.; Brabec, V.; Marchán, V. Towards Novel Photodynamic Anticancer Agents Generating Superoxide Anion Radicals: A Cyclometalated Ir(III) Complex Conjugated to a Far-Red Emitting Coumarin. *Angew. Chem., Int. Ed.* **2019**, *58*, 6311−6315.

(42) Warren, J. J.; Tronic, T. A.; Mayer, J. M. Thermochemistry of Proton-Coupled Electron Transfer Reagents and its Implications. *Chem. Rev.* **2010**, *110*, 6961−7001.

(43) Lin, H.; Chen, Y.; Shi, J. Nanoparticle-triggered in situ catalytic chemical reactions for tumour-specific therapy. *Chem. Soc. Rev.* **2018**, *47*, 1938−1958.

(44) Searle, P. F.; Chen, M.-J.; Hu, L.; Race, P. R.; Lovering, A. L.; Grove, J. I.; Guise, C.; Jaberipour, M.; James, N. D.; Mautner, V.; Young, L. S.; Kerr, D. J.; Mountain, A.; White, S. A.; Hyde, E. I. NITROREDUCTASE: A PRODRUG-ACTIVATING ENZYME FOR CANCER GENE THERAPY. *Clin. Exp. Pharmacol. Physiol.* **2004**, *31*, 811−816.

(45) Huang, H.; Yu, B.; Zhang, P.; Huang, J.; Chen, Y.; Gasser, G.; Ji, L.; Chao, H. Highly Charged Ruthenium(II) Polypyridyl Complexes as Lysosome-Localized Photosensitizers for Two-Photon

Photodynamic Therapy. *Angew. Chem., Int. Ed.* **2015**, *54*, 14049−14052.

(46) Huang, C.; Liang, C.; Sadhukhan, T.; Banerjee, S.; Fan, Z.; Li, T.; Zhu, Z.; Zhang, P.; Raghavachari, K.; Huang, H. In-vitro and In-vivo Photocatalytic Cancer Therapy with Biocompatible Iridium(III) Photocatalysts. *Angew. Chem., Int. Ed.* **2021**, *60*, 9474−9479.

(47) Luo, Z.; Yuan, X.; Yu, Y.; Zhang, Q.; Leong, D. T.; Lee, J. Y.; Xie, J. From aggregation-induced emission of Au(I)-thiolate complexes to ultrabright Au(0)@Au(I)-thiolate core-shell nanoclusters. *J. Am. Chem. Soc.* **2012**, *134*, 16662−16670.